Proc. of the 8th International Symposium on Geotechnical Safety and Risk (ISGSR)
Edited by Jinsong Huang, D.V. Griffiths, Shui-Hua Jiang, Anna Giacomini and Richard Kelly
 Published by Research Publishing, Singapore.
doi: 10.3850/978-981-18-5182-7_11-011-cd

ISGSR 2022

Catastrophic Landslide Triggered by Extreme Rainfall in Chongqing, China: July 13, 2020, Niuerwan Landslide

Chang Zhou[1], Wei Huang[*2]

[1]School of Resources and Geosciences, China University of Mining and Technology, Xuzhou, Jiangsu, P.R. China.
E-mail: changzhou@cumt.edu.cn
[2]The Seventh Geological Brigade of Hubei Geological Bureau, Yichang, Hubei, P.R. China
E-mail: huangwei@cug.edu.cn

Abstract: At approximately 7:00 a.m. (Beijing time) on July 13, 2020, a catastrophic soil and rock landslide occurred in Baima Town, Wulong District, Chongqing, China. With a length of 750 m and a width of 125m to 260 m, the landslide carried approximately 1.4×10^6 m3 of rock and soil debris and destroyed eight houses, two main roads, a shale gas pipeline, and a large amount of farmland. Field investigation found that the reactivated deposits were still moving. The failure mechanism of the landslide was analyzed based on the geological conditions, deformation process and triggering factors. The research shows that the Niuerwan landslide had a complex deformation process. According to the deformation characteristics, the landslide was divided into five parts: the source area, the compression area, the rapid sliding area, the landslide-affected zone and the accumulation area. The source area was triggered by continuous torrential rainfall and controlled by mudstone and bedding plane. The variation of the microrelief in the study area has significant effect on the failure model of the landslide. Precipitation increased the weight of the sliding mass by saturating the soil and rocks, and the shear strength was decreased by water erosion. Consequently, the steep source area firstly deformed and impacted the middle part. Eventually, a continuous sliding surface developed along the weak layer, giving rise to catastrophic failure. Moreover, the accumulation area at the steep slope toe rapidly moved downward to form a debris flow under the combined action of the geological conditions and rainfall. The Niuerwan landslide is a complex rainfall-induced landslide with a unique evolution process, which can provide a reference for landslide disasters.

Keywords: Rainfall; deformation characteristics; failure mechanism; debris flow; Evolution process

1 Introduction

Landslides are among the most severe geohazards in mountainous areas (Wu et al, 2015; Salvati, et al, 2015; Froude et al, 2018; Zhang et al, 2018). Many triggers may cause catastrophic landslide failures, such as rainfall, reservoir operations, earthquakes and other external factors (Radbruch et al, 1976; Keefer, 1984; Alexander, 1992; Zhou et al, 2017; Zhou et al, 2018). Some studies have found that seasonal and torrential rainfalls trigger landslides by increasing the pore water pressure inside landslide masses (Vita et al. 1998; Tsai 2008; Li et al, 2018). In particular, the mudstone strength and elastic modulus decrease rapidly with increasing water content (Huang et al, 2008; Wen et al, 2012; Zhang et al, 2016).

On July 13, 2020, a catastrophic landslide mass (the No. 2 Niuerwan landslide) occurred in Chongqing city after continuous heavy rainfall. The landslide destroyed eight houses, two main roads, a gas pipe and farmlands. Additionally, the potential landslide area and the slipped area deposits still have the potential to fail. After the failure of the Niuerwan landslide, an emergency investigation was carried out. Landslide mapping and estimation of the dimensions were carried out via drones. The deformation characteristics of the landslide surface during the failure process were collected through local residents' reports. The deformation process of the Niuerwan landslide was divided into four stages. Finally, the failure mechanism of the landslide was analyzed, and the stability of the Niuerwan landslide was reevaluated.

2 Geological settings

The Niuerwan landslide is located in Baima town, Wulong District, Chongqing city (N29°24′01", E107°30′44"), approximately 144 km from Chongqing city (Figure 1). Two rivers, namely, the Shiliang and Wujiang Rivers, are approximately 1.5 km and 2.0 km from the landslide, respectively. Chongqing City has a subtropical monsoon climate with an annual. The rainfall data from June to September are shown in Figure 2. The rainfall in June 2021 before the landslide was 250 mm, which is 2.86 times of the same year, and 2.29 times of the highest value of 109 mm (July) in the 1975-2020. The monthly rainfall in July 2021 reached 402 mm, 313 mm more than that in the same year.

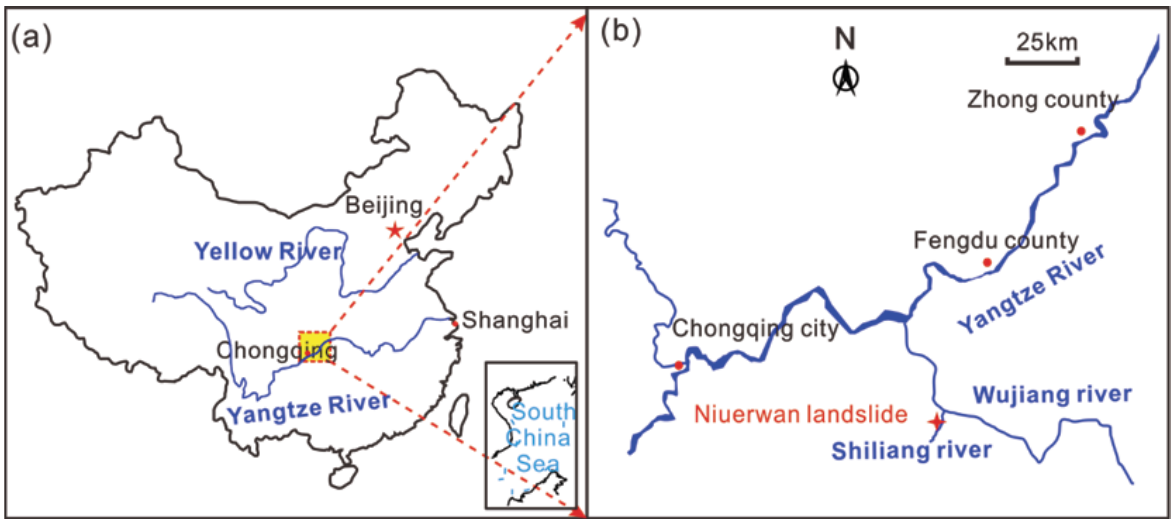

Figure 1. The location of the Niuerwan landslide

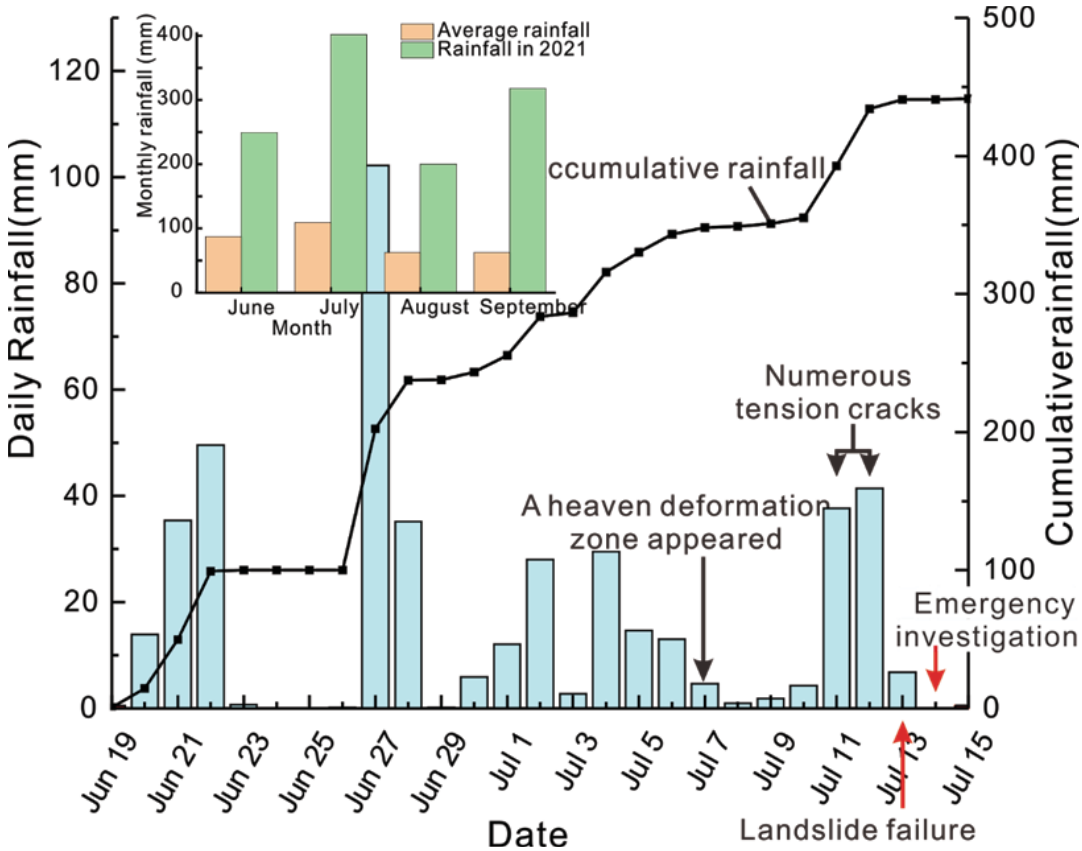

Figure 2. Daily rainfall and monthly rainfall in the Niuerwan landslide

The local regional landscape is mainly mountainous. The Niuerwan landslide is located in the west wing of the Baima syncline. the steep, gentle and steep micro-geomorphology are developed in the landslide area (Figure 3, Figure 4). Field investigations found that the main geological units in the study area are surficial deposits and sedimentary bedrock (Figure 3). The surficial deposits are usually capped by eluvium and colluvium. The eluvium is mainly composed of silty clay and 15% - 22% gravel clasts. The diameters of the gravel clasts range from 10 mm to 250 mm. The permeability of the loose gravel soils is 6.2 $\times 10^{-4}$ m/s to 5.2 $\times 10^{-3}$ m/s, which is considerably high, as determined by water injection tests. The bedrock is thinly layered purplish red mudstone of the Leikoupo Formation of the mid-Triassic system (T_2^l). The bedrock dips 15° - 22° toward 110° -125° (Figure 3b). Fractures in the mudstone layers have developed, and there are two sets of dominant fractures in the mudstone layer. The first fracture dips 65° toward 30°. Its spacing is 0.5-2.0 m and is 0.6-1.0 m long and 2-10 mm wide. The second fracture dips 76° toward 310° with a length and width of 0.4-1.5 m and 2-8 mm, respectively. Its spacing is 0.6 - 3.0 m.

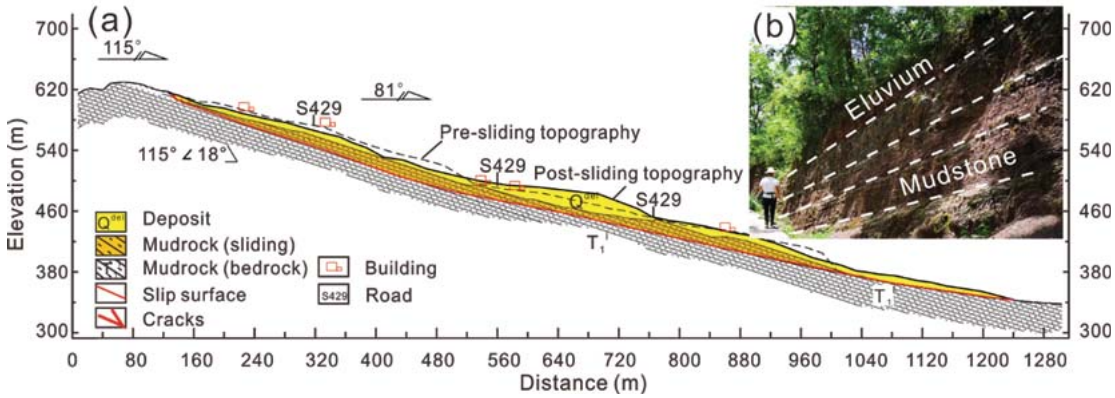

Figure 3. The profile section of the landslide along the 1-1` in Fig. 2b, b) eluvium and mudstone.

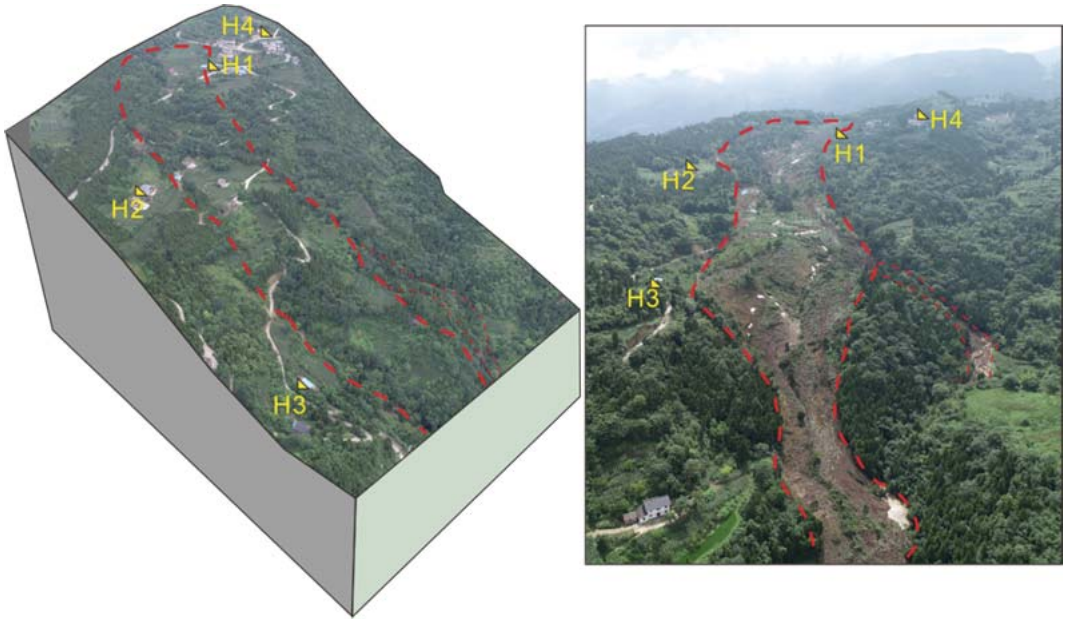

Figure 4. Three-dimensional topographic maps of the landslide area

The unmanned aircraft used in this paper is FEIMA D200 produced by FEIMA Robotics company. This equipment has High-precision differential GNSS module and its' software system has many function such as route design, flight operation, data calculation, etc. This paper obtained 3678 pieces of optical image data, one set of POS data. The main features of the FEIMA D200 unmanned aircraft are shown in Table. 1.

Table 1. The main features of the FEIMA D200 unmanned aircraft

Project	Specifications	Photograph
Weight	6.5kg	
Size	830×732×378mm	
Loadable weight	< 3.5kg	
Duration	48 min	
Speed	36～54km/h	
Maximum Elevation Angle	25°	
hovering accuracy RTK	Horizontal: 1cm+1ppm; Vertical: 2cm+1ppm	
wind resistance capability	5 scale	

3 Deformation characteristics

3.1 Deformation history

In 1998, several cracks were found on the uphill side of the Niuerwan landslide by residents, so they were recorded

in the Geo-Hazards Mitigation System by Residents' Self-Understanding and Self-Monitoring in 2000, which focused on the deformation of the landslide surface recorded by residents.

After 1998, no obvious deformation occurred in this landslide. However, in 2020, heavy rainfall caused catastrophic floods in southern China. The Niuerwan landslide began to deform after continuous rainfall (Figure 2). Residents reported that a tension deformation zone was found upside of the landslide on July 7, 2020 (Figure 5). The length, width and thickness of the initial deformation zone were approximately 200 m × 100 m × 15 m, respectively, and its maximum vertical displacement was 30 mm. Shear cracks formed on the two sides of the landslide with a width of 150 mm (Figure 5ae). The road in the middle-lower area slipped more than 100 mm. Under the effect of the heavier rainfall (more than 37 mm/day) on July 11-12, the landslide had obvious deformation from July 12 to 5:00 am on July 13 (Figure 5bcf), and numerous arc tension cracks were found in the uphill slope with a maximum vertical displacement of 0.3 m -1 m and an average width of 0.2 m. The shear cracks gradually expanded in length and width, and their widths increased to 0.3 m -2 m. As a result, the road slipped 0.5 m -5.0 m (Figure 5gh). Moreover, a crack 600 m long and 100 mm-170 mm wide traversed the landslide. Then, the sliding surface traversed the landslide (Figure 5d), and the landslide failed at approximately 7:00 a.m. on July 13. Numerous cracks were generated in the landslide (Figure 5i). The maximum vertical displacement of the upside slope was approximately 1.5 m. Field investigation found that the reactivated deposits were still moving. The road debris in front of the landslide moved over 150 m during July 14 to July 30.

Figure 5. Deformation process of the road on the upper part of the landslide at different times. a-c tensile cracks on the north boundary of the landslide; d photo of cracks in front of the landslide; e-g tensile cracks on the south boundary of the landslide at different times. h photo of the road on the landslide.

3.2 Deformation characteristics of the Niuerwan landslide

In plain view, the Niuerwan landslide has an irregular shape, with the length and width of the landslide being 900 m × 200 - 470 m, respectively (Figure 6b). The average thickness of the landslide is approximately 10 m. The principal sliding directions of the upper and middle-lower parts are approximately 115° and 81°, respectively. The boundaries of the landslide are very clear. The southern boundary is the mountain ridge, the northern boundary is a tension valley, and the upper boundary is the summit of the mountain. The valley, with a length of approximately

2.5 km and width of 5 – 20 m, connects with the Shiliang River. According to the deformation characteristics, the Niuerwan landslide could be divided into the source area (Zone A), the compression area (Zone B), the rapid sliding area (Zone C), the landslide-affected area (Zone D) and the accumulation area (Zone E, F) (Figure 7).

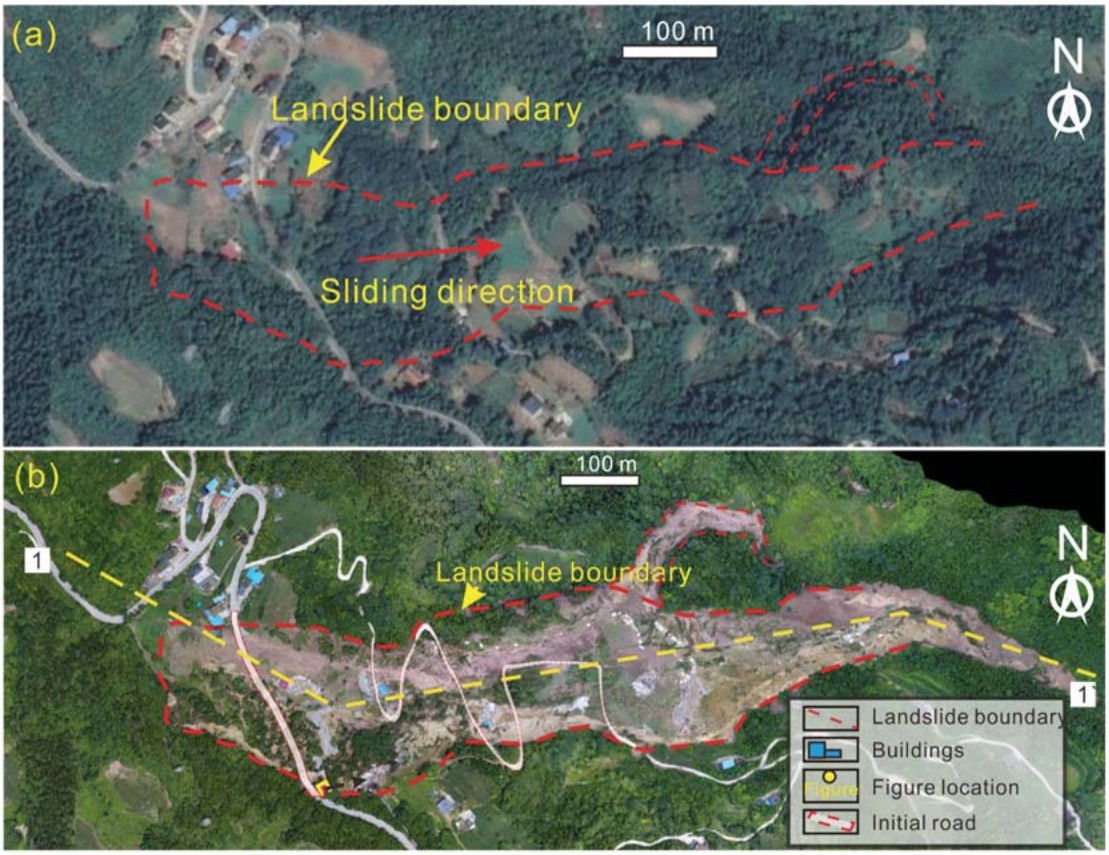

Figure 6. Plan view of the Niuerwan landslide before and after failure. a) Google Earth Image on Sep 2, 2019; b) unmanned aircraft image after the landslide (July 30, 2020)

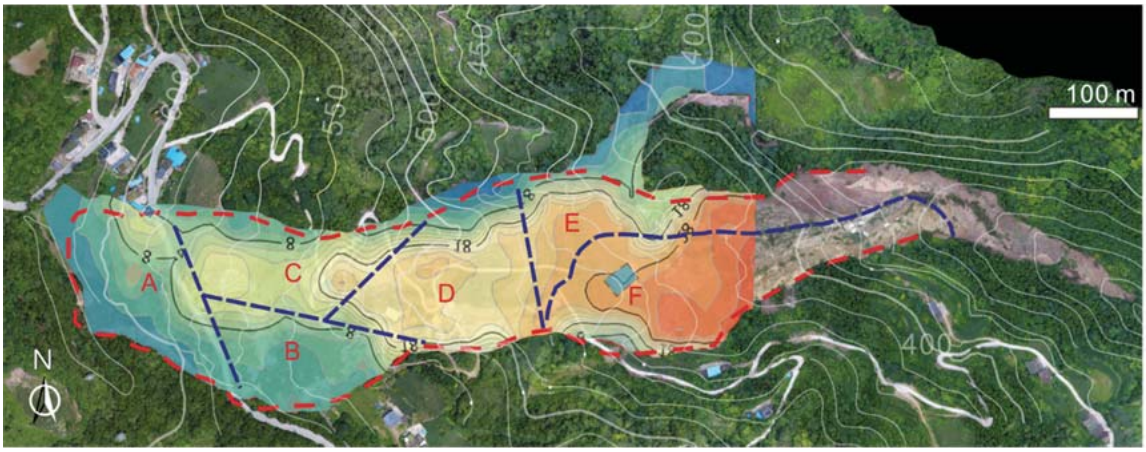

Figure 7. Post-landslide topography and displacement. A-F mark the zone of the landslide.

3.2.1 Source area (Zone A)

The source area is at elevations of 560 m- 615 m (Figure 8). This area is 40 m -190 m wide, 250 m long, and 15.0 m – 20.0 m thick (Figure 8c). The landslide volume of the source area is approximately 2.4×10^4 m^3. Numerous arc tension cracks were found in the upper part of the source area with a maximum vertical displacement of 0.3 m -1 m (Figure 8abce). The sliding scratches on the landslide scarp and the sliding zone are clear (Figure 8df). The sliding direction of the source area was changed by the mountain at the southern boundary, which in turn caused a number of sabre trees to be generated. The road was destroyed (Figure 8c). On the source area, the displacement of the northern part was larger than that of the southern part.

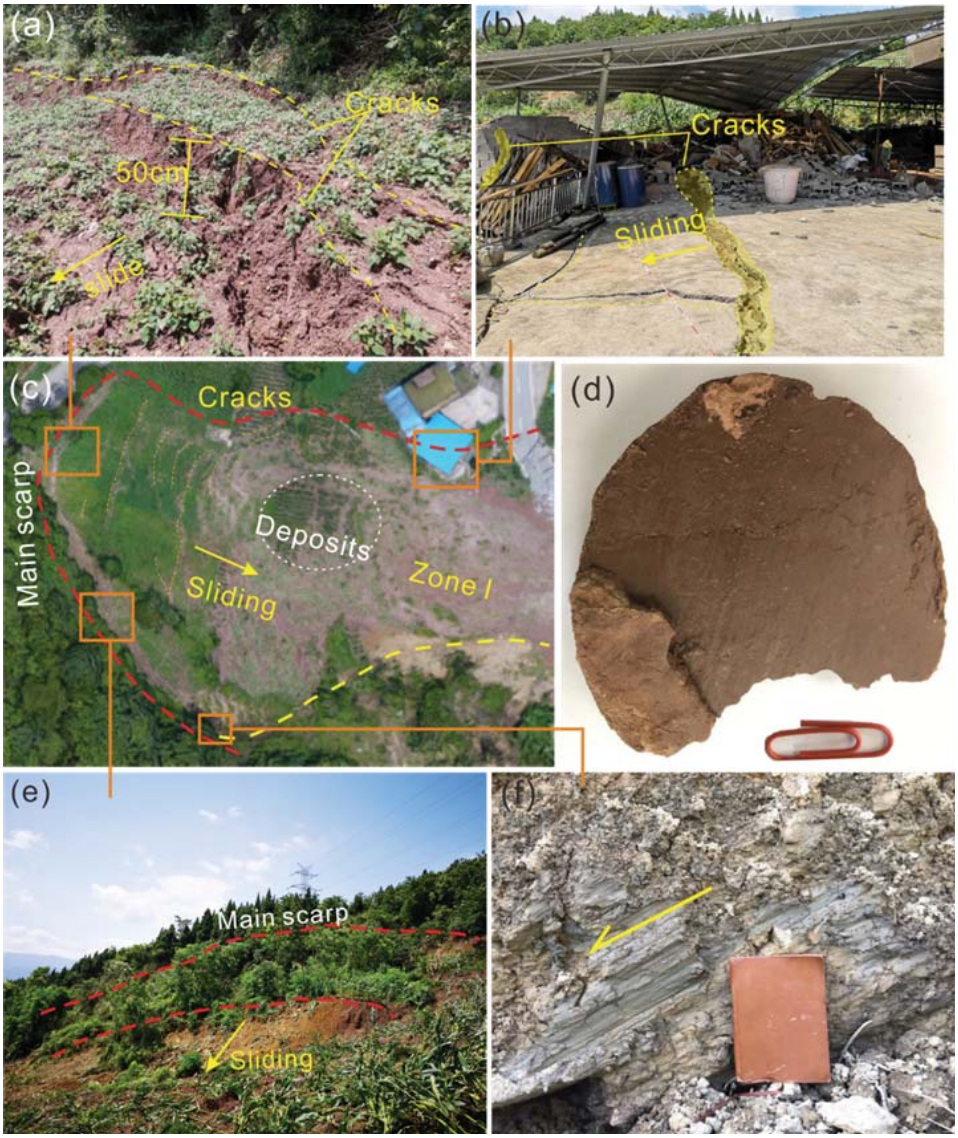

Figure 8. Photos of the source area (Zone A); a b e) the boundary of the landslide; c) the main scarp of the landslide; d the slip scratches on the sliding zone; f the slip scratches in the trailing edge of the landslide

3.2.2 Compression area (Zone B)

The compression area (Zone B) is located below the source area at elevations of 500 m -560 m (Figure 9a). The sliding of the source area impacted this area, and some vertical tensional and shear cracks formed at this area because of the blocking of the terrain (Figure 9bde). Besides, the south boundary of the compression area was obvious, and its maximum vertical displacement was 5 m -10 m (Figure 9f). Many gray broken mudstones (0.5 - 1.5 m diameter) were found in front of this area (Figure 9c). The sliding direction of the source area was changed by the mountain at the southern boundary.

Figure 9. The compression zone (Zone B) and rapid-sliding zone (Zone C) of the Niuerwan landslide. a) the location of the compression zone; b) d the deformation of the road S529; c) the gray broken rocks; de) the photo of the broken building; f) the main scarp on the south boundary of the landslide

3.2.3 Rapid-sliding zone (Zone C)

The rapid-sliding zone is located below the source area (Figure 4 and Figure 9a). This area deformed as the source area deformed. When the landslide failure, the rapid-sliding zone slid over 10 m at high speed, and impacted the landslide-affected zone.

3.2.4 Landslide-affected zone (Zone D)

The landslide-affected zone is located between zone B and C at elevations of 480 m – 536 m (Figure 10 ac). The reactivated deposits of zone A and B are accumulated on both side of this zone (Figure 10b). The slope of the landslide-affected zone is approximately 120 which is smaller than that of resource area (200) before landslide. The accumulation shape in July 13 is triangular and the slope decreased to 90.

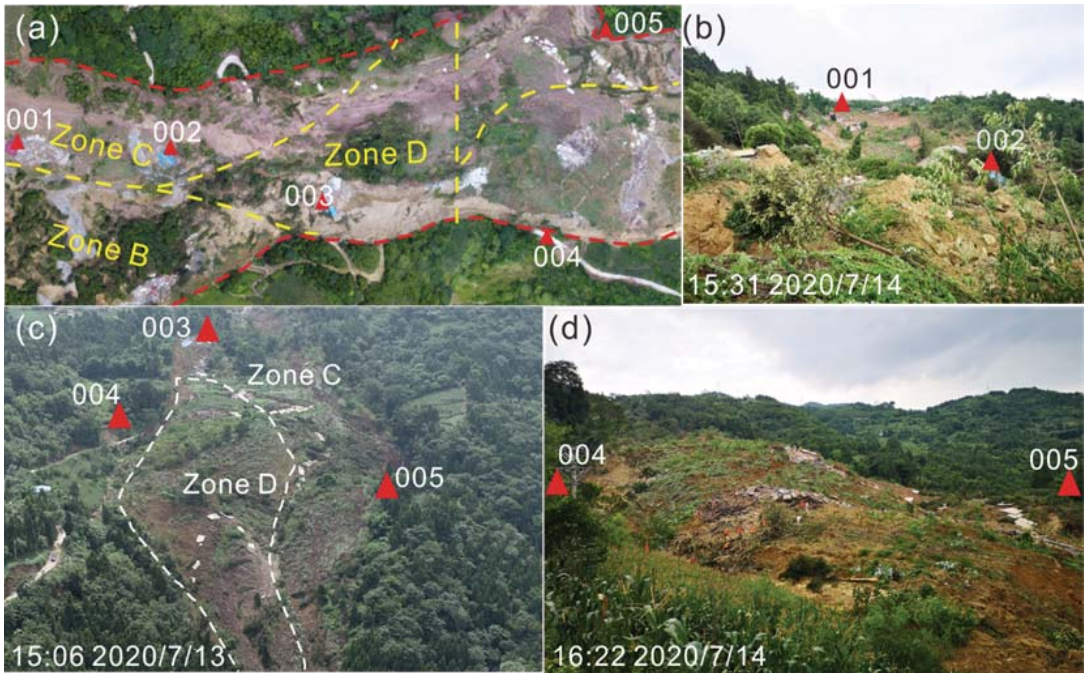

Figure 10. Photos of the middle part of the landslide photographed by inspectors, with photo time and reference building marked on the photos; a) the vertical view; b) an overview of the middle part; c-d) photos of the accumulation area.

3.2.5 Accumulation area

According to the source of the deposits, the accumulation area can be divided into Zone E and F (Figure 11ac). Zone E is located in the north side of the accumulation area, below the landslide-affected area. The clay of the Zone E is reddish-brown and it was divided into two parts by a hill, forming a human-shape. The Zone F is located in the south side of the accumulation area (Figure 10d). The clay of the Zone F is mix reddish-brown and yellow (Figure 11bd). After landslide occurred in July 13, the accumulation area still moved by comparing the location of the road debris at different time (Figure 10a c).

The slope of the accumulation area increased, but the cross-section rapidly decreased, so that the deposits rapidly slid and formed a debris flow area (Figure 11ac). This area was located in the downslope. The deposits in this area were mainly composed of clay. The clay layer moved as debris flow under the effect of the rainfall, and it was divided into two parts by the hill' obstruction: Most of them slipped forward over 100m along the main sliding direction. The location of road debris suggested that the different portion of the landslide had different deformation. Moreover, water seepage phenomena were found at the slope toe (Figure 11b de), so that the deposits at the slope toe slid over 200 m. However, the accumulated deposits are loose and has relatively lower water content (approximately 12%).

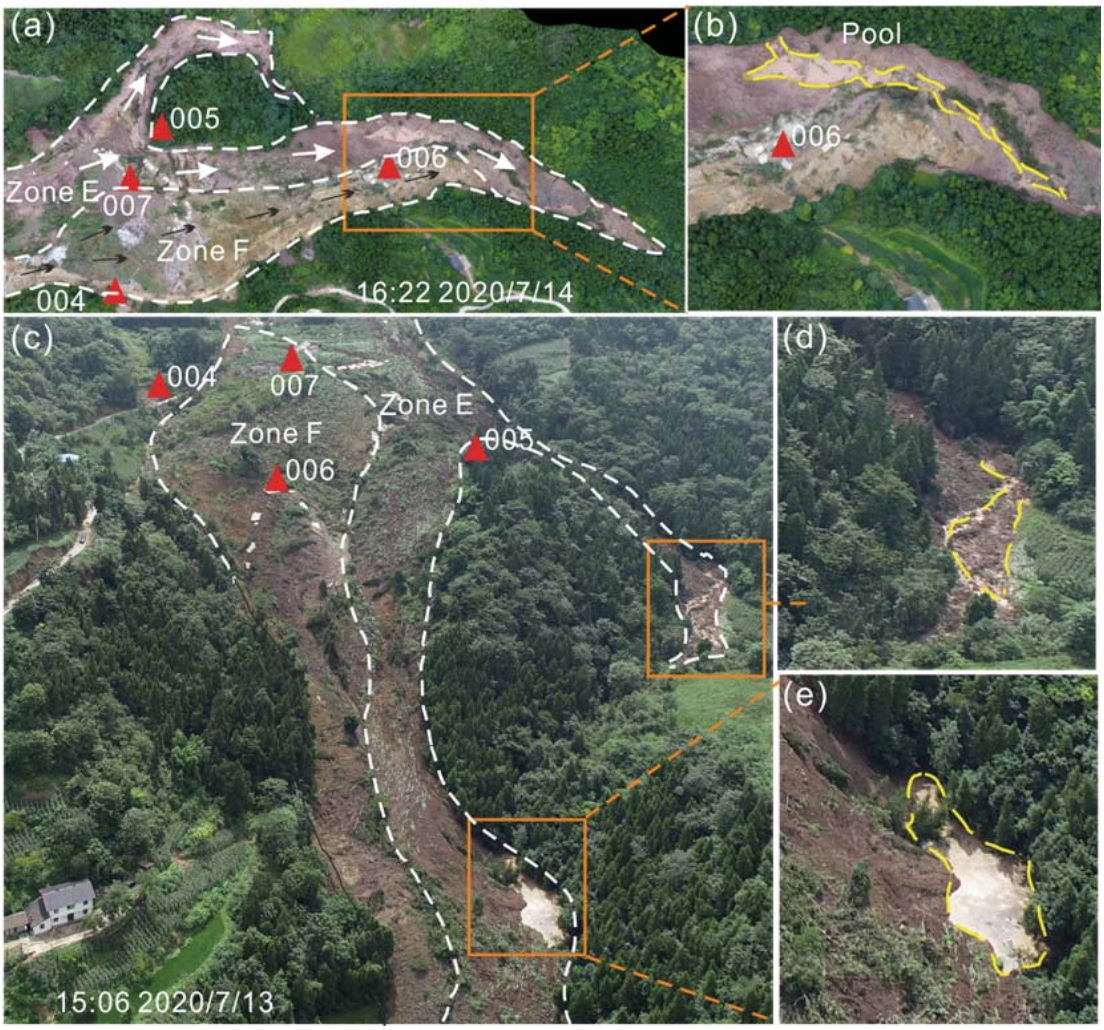

Figure 11. The accumulation area of the Niuerwan landslide. a) the vertical view; b d- e) water seepage at the slope toe; c) the front view

4 Predisposing factors and trigger

4.1 Geomorphic property

The average slope of the Niuerwan landslide is approximately 16°. The slope of the upper, middle and lower part of the landslide is approximately 20°, 12° and 28°, respectively. The steep source area provides conditions for landslide instabilities. The middle part of the landslide is gentle, which provides a platform for the landslide accumulation. The steep and narrow toe of the landslide provides conditions for the debris flow movement.

4.2 Geological properties

Field investigations indicated that the mudstone developed vertical fractures that provided channels for rainfall infiltration. Moreover, under the effect of soil-water interactions, the shear strength of mudstone decreases dramatically (Wen et al, 2012; Wang et al, 2015; Zhang et al, 2016). Therefore, after continuous heavy rainfall, the structure and strength of the mudstone could have decreased, which may have explained why the landslide slid along the weak layer in the bedrock. Moreover, the sliding direction of the upper part of the landslide at elevations of 480 m – 615 m is 115°, which is roughly the same as the dip direction of the bedrock (110 - 125°). In this part, the potential sliding surface was generated along the bedding plane. However, at the elevations of 380 m – 480 m, the sliding direction of the landslide changed from 115° to 81°, and the slope of the sliding surface changed from 20° to 13°. Therefore, there was an intersection angle between sliding surface and bedding plane, which increased the stability of the landslide. The dominated fracture (30°∠65°) controlled the south boundary of the landslide, which provides the necessary geological conditions for the formation of the landslide.

4.3 Continue intensity rainfall

In 2020, heavy rains caused amounts of catastrophic floods and geohazards in China. Figure 2 shows that from June to September, 2020, the rainfall in the study area was obviously higher than that in previous years. On June

27 – 28, there was strong rainfall (with an accumulation of 137 mm), and then continuous intense rainfall occurred after June 30 before the landslide had obvious deformation. On July 11 -12, there was another continuous rainfall (over 40 mm/day) occurred, and the deformation of the source area accelerated. The Niuerwan landslide occurrence didn't obvious lag rainfall. First, the rainfall infiltrated into the landslide and increased the water content of the landslide. As a result, the weight of the sliding mass was increased. Second, cracks expanded due to the water pressure, which was induced by rainfall infiltration. In addition, the water content played an important role in the strength of the mudstone.

4.4 The secondary landslide caused by impact liquefaction

The soil structure could be destroyed and the soil pressure rapidly increases under vibration load (Dun et al., 2020; Rahmani et al., 2020). As results, the sliding zone soil is completely saturated, and the shear strength decreased. Eventually, the liquefaction of the saturated soil occurred and the sliding mass soil moved to form a debris flow (Yi et al., 2021). In the Niuerwan landslide, the deformation of the landslide mainly concentrated on the upper part of the landslide (Zone A, B and C) before the landslide occurred. Therefore, gravity potential energy was transformed to the kinetic energy, and the upper part of the landslide impacted the landslide-affected area (Zone D), causing the high-speed downward sliding. The fact can be confirmed by the loose deposits and the obvious water seepage at the landslide toe (Figure 11).

In conclusion, continuous torrential rainfall triggered the upstream of the landslide, so that the upstream of the landslide accelerated along the mudstone layer after torrential rainfall from July 11 to July 12 because tension cracks and steep slope accelerated the rainfall infiltration. However, the middle part of the landslide didn't have large deformation because of the intersection angle between the sliding surface and mudstone layers. As the source area deformed, the potential sliding surface gradually traversed the landslide and the landslide occurred. The potential energy was rapidly released, and the landslide tend to stable. However, reactivated deposits still are moving forwards under continuous heavy rainfall.

5 Deformation process of the landslide

The Niuerwan landslide occur because of a combination of geological and rainfall factors. According to the deformation history, the deformation process of the landslide was divided into four stages (Figure 12, Figure 13).

(1) Initial deformation stage (1998 to July 6, 2020, Figure 12a): Several cracks were found in the upstream side of the landslide in 1998, which could be caused by the increase of water content and pore water pressure of the sliding zone, and then the landslide tends to stable. This fact can be confirmed by the sabre trees at the source area.

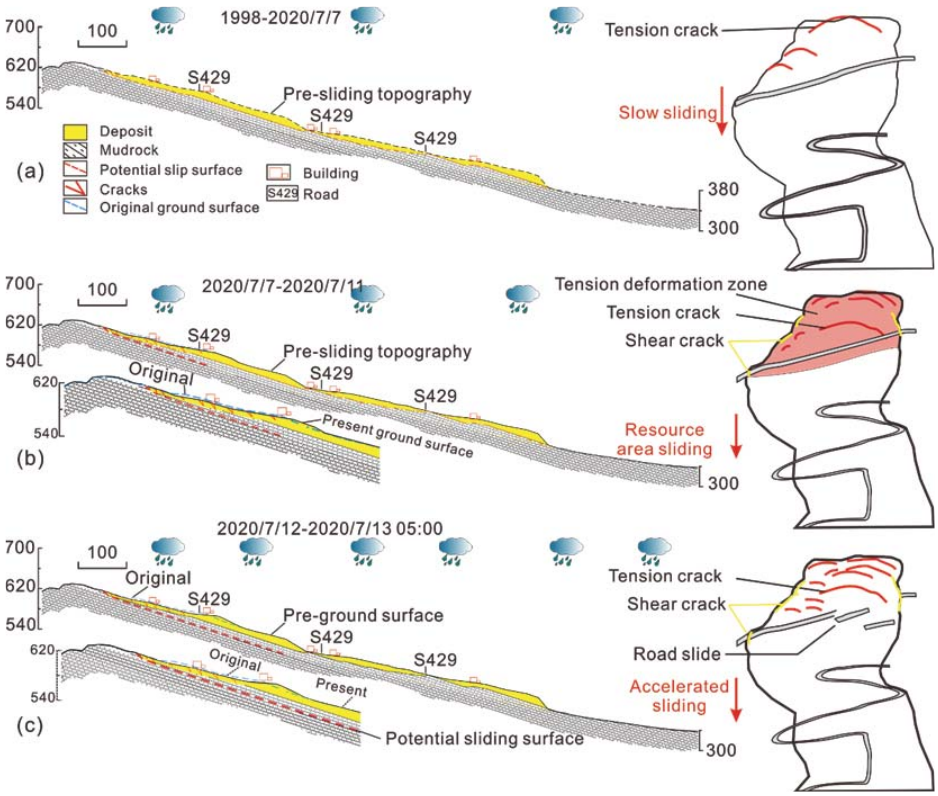

Figure 12. Conceptual model of the evolution process of the Niuerwan landslide. a) initial, b) local damage, c) accelerated deformation stage

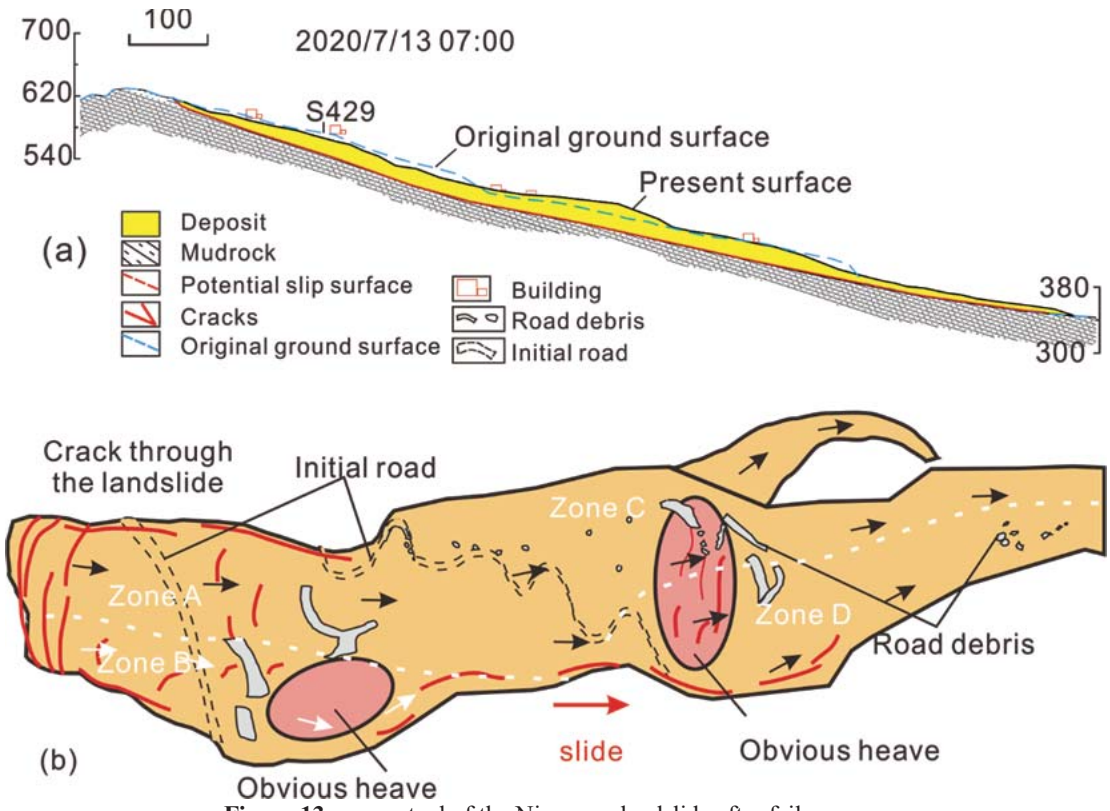

Figure 13. conceptual of the Niuerwan landslide after failure

(2) Local damage at the rear section of the landslide (July 7, 2020 to July 11, Figure 12b): Rainfall rapidly infiltrates into the sliding mass, and increase the water content and the pore water pressure. As results, the shear strength of the weak layer decreased, and the weight increased. The steep geomorphology provides good geomorphic conditions for the source area failure. Therefore, a tensile stress area appeared and some tension cracks formed under the gravity effect. The potential sliding surface generated along the bedding plane.

(3) Accelerated deformation stage (July 12 to 5:00 a.m. July 13, Figure 12c): These cracks on the surface provided seepage channel for rainwater, which in turn caused the cracks to expand in length and width, and connect. The rear part of the landslide rapidly deformed and impacted the middle portion. The source area boundary gradually formed. However, due to the buffer of the gentle slope platform and rock layer that intersect with potential sliding surface, the deformation was concentrated on the upper part of the landslide.

(4) Failure stage (7:00 a.m., July 13, 2020, Figure 11): The sliding of the upper part of the landslide impacted the landslide-affected zone. The sliding surface developed through the landslide. The landslide had suddenly large displacement. The road and buildings damaged. The reactivated deposits were mainly accumulated in the middle-lower area.

(5) Debris flow stage: Under the effect of continuous rainfall and gravity, the loose deposits at the slope toe continued to move and formed a debris flow. The deposits of the source area slowly moved downward.

6 Conclusion

The geological conditions, deformation characteristics and triggering factors of the Niuerwan landslide in Chongqing, China are introduced. The landslide was reactivated on July 7, 2020, accelerated and failed on July 13, responding to continuous intense rainfall. The failure mechanism of the Niuerwan landslide was revealed. The deformation of the steep source area accelerated along the bedding plane and impact the middle part of the landslide, causing secondary sliding. The accumulation area rapidly moved downward to form a debris flow because of the steep slope toe and the reduction of the cross-section. As results, the landslide damaged eight houses, two main roads, a shale gas pipeline.

The Niuerwan landslide exhibited a complex failure mechanism which was controlled by the geology, the topography and the intense rainfall. The bedding plane provided a potential sliding surface of the source area but played a buffering role for the middle part of the landslide. Moreover, the steep, gentle and steep micro-geomorphology controlled the deformation model of the landslide. The soften and scour of rainwater destroyed the structure of mudstone, and decreased the strength, so that a tension stress area appeared in the upper slope. Tension cracks provided seepage channels for rainfall, which in turn, caused the cracks to expand rapidly. The steeper resource area in the trailing edge of the landslide began to deform and compress the middle portion, finally failed. According to the deformation characteristics, the deformation process of the Niuerwan landslide is divided into five stages: initial, local damage, acceleration, failure and debris flow stage.

Declarations

Funding

The author sincerely acknowledges the support from This study was financially supported by the Fundamental Research Funds for the Central Universities (2021QN1082); Key Research and Development Program of Xinjiang Uygur Autonomous Region (Grant No. 2021B03004-3);

Conflicts of interests

The authors declare that they have no known competing financial interests or personal relationships that could have appeared to influence the work reported in this paper.

Reference

Alexander D., (1992). On the causes of landslides: human activities, perception, and natural processes. *Environmental Geology*, 20(3):165-179.

Duan, Z., Dong, C., Zheng, W., Tang, H., Ma, J., (2020). liquefaction mechanism of terrace sandy silt under landslide impact. *Journal of Engineering Geology*, 28(6):1362–1371.

Froude, M.J., Petley, D., (2018). Global fatal landslide occurrence from 2004 to 2016. *Natural Hazards and Earth System Sciences*, 18: 2161-2181.

Huang, R.Q., Zhao, S.J., (2008). Formation and mechanism analysis of Tiantai landslide, Xuanhan County, Sichuan Province. Proceedings of the 10th International Symposium on Landslides and Engineered Slopes, 30 June-4 July 2008, Xi'an, China. *Landslides and Engineered Slopes: From the Past to the Future*, 32(1), pp. 1171–1181.

Keefer, D.K., (1984). Landslides caused by earthquakes. *Geological Society of America Bulletin*, 95(4): 406-421.

Li, C.R., Wang, M., Liu, K., 2018. A decadal evolution of landslides and debris flows after the Wenchuan earthquake. *Geomorphology*, 323: 1-12.

Radbruch, D.H., Varnes, D.J., (1976). Landslides-cause and effect. *Bulletin of the International Association of Engineering Geology*, 13: 205-216.

Rahmani H, Naeini S., (2020). Influence of non-plastic fine on static liquefaction and undrained monotonic behavior of sandy gravel. *Engineering Geology*, 275:105729.

Salvati, L., Carlucci, M., (2015). Towards sustainability in agro-forest systems? Grazing intensity, soil degradation and the socioeconomic profile of rural communities in Italy. *Ecological Economics*, 112: 1–13.

Tsai TL. (2008). The influence of rainstorm pattern on shallow landslide. *Environmental Geology*, 53(7): 1563-1569.

Vita, P.D., Reichenbach, P., Bathurst, J.C., et al., 1998. Rainfall-triggered landslides: a reference list. *Environmental Geology*, 35(2): 219-233.

Wang, L.L., Bornert, M., Héripré E, Chanchole, S., et al., (2015). The Mechanisms of Deformation and Damage of Mudstones: A Micro-scale Study Combining ESEM and DIC. *Rock Mechanism and Rock Engineering*, 48: 1913-1026.

Wen, B.P., He, L., (2012). Influence of lixiviation by irrigation water on residual shear strength of weathered red mudstone in Northwest China: implication for its role in landslides' reactivation. *Engineering Geology*, 151: 56–63.

Wu, X.L., Chen, X.Y., Zhang, F.B., (2015). Global research trends in landslides during 1991–2014: a bibliometric analysis, 12: 1215-1226.

Yi, X. and W. Feng, et al., (2021). Catastrophic landslide triggered by persistent rainfall in Sichuan, China: August 21, 2020, Zhonghaicun landslide. *Landslides* 18(8): 2907-2921.

Zhang, S., Xu, Q., Hu, Z.M., (2016). Effects of rainwater softening on red mudstone of deep-seated landslide, Southwest China. *Engineering Geology*, 204: 1-13.

Zhang, Y.M., Hu, X.L., Dwayne, D.T., et al., (2018). Field monitoring and deformation characteristics of a landslide with piles in the Three Gorges Reservoir area. *Landslides*, 15: 581-592.

Zhou, C., Hu, X.L., Xu, C., et al., (2018). Model test on deformation and failure of landslide in water-level-fluctuating zone of Three Gorges Reservoir region. *China Journal of Highway and Transport*, 31(2): 252-260.

Zhou, J.W., Jiao, M.Y., Xing, H.G., et al., (2017). A reliability analysis method for rock slope controlled by weak structural surface. *Geosciences Journal*, 21 (3): 453-467.